2026 IEEE/SICE International Symposium on System Integration (SII)
January 11-14, 2026. Cancún, México

Study on Roller-Walker: Development of Roller-Walker II Using 3D Printed Structural Components

Hana Ito[1], Akifumi Okubo[1], Kurumi Osawa[1], Takahiro Aruga[1], and Gen Endo[1]

***Abstract*— We developed Roller-Walker II, a leg-wheeled hybrid robot that primarily uses 3D-printed plastic as its structural material. This robot achieves both walking and wheel-based locomotion called "Roller-Walk" by rotating its ankle joints 90 degrees to switch between different foot configurations. The ankle switching mechanism also employs 3D-printed lead screws, realizing a compact, lightweight, and high load-bearing capacity mechanical configuration. Locomotion experiments were conducted for both walking and Roller-Walk modes, confirming that the robot can successfully propel itself in both modes without issues. Particularly in Roller-Walk mode, the robot achieved a maximum velocity of 3.43 m/s and a CoT of 0.14, placing it among the group of walking robots with the highest mobility performance when compared to other walking robots.**

I. Introduction

In recent years, the development of walking robots capable of moving on rough terrain has been actively pursued [1], and their deployment for purposes such as exploration and transportation in real-world environments has begun [2] [3]. However, on hard flat terrain, walking robots have the disadvantage of lower moving speed and lower mobility efficiency compared to wheeled robots. Therefore, leg-wheeled robots that combine both legs and wheels have been developed [4] [5] [6] [7] [8]. However, such leg-wheeled robots typically have actuators attached to the leg tips to drive the wheels, which makes the mechanism large and heavy, resulting in the disadvantage of degraded walking performance. To address this issue, Endo et al. developed a leg-wheeled robot called Roller-Walker [9], which attaches passive wheels that also serve as foot soles to the tips of four legs and performs wheel locomotion using the same degrees of freedom as walking legs by rotating the ankle joints 90 degrees to switch to wheels. This propulsion method is called Roller-Walk. The only addition required to achieve both walking and Roller-Walk is the ankle switching mechanism, which is more compact and lightweight compared to wheel-driving actuators. Therefore, it is possible to achieve both walking and wheel-based locomotion without degrading walking performance. To further pursue weight reduction and higher power output, we considered developing the Roller-Walker using 3D-printed plastic components.

Many robots using 3D-printed plastic components have been developed previously [10] [11] [12] [13], and TITAN-E1 [14] developed by our research group is one such example. However, the significantly lower strength of plastic compared to metal remains a challenge. In fact, in TITAN-E1, large tensions applied by timing belts used for joint actuation and ropes for coupled tendon drive caused significant deformation and cracks that resulted in delamination along the layer direction. This ultimately led to the robot's failure to operate normally. Therefore, in this study, we developed Roller-Walker II shown in Fig. 1, aiming to prevent deformation and cracking even when using 3D-printed plastic components as the primary structural material. Focusing on the compact and lightweight characteristics of the leg tips, which are features of the aforementioned Roller-Walker, we aimed for an even more lightweight and simple configuration for the ankle switching mechanism. This paper describes the design of Roller-Walker II and the operations of walking and Roller-Walk.

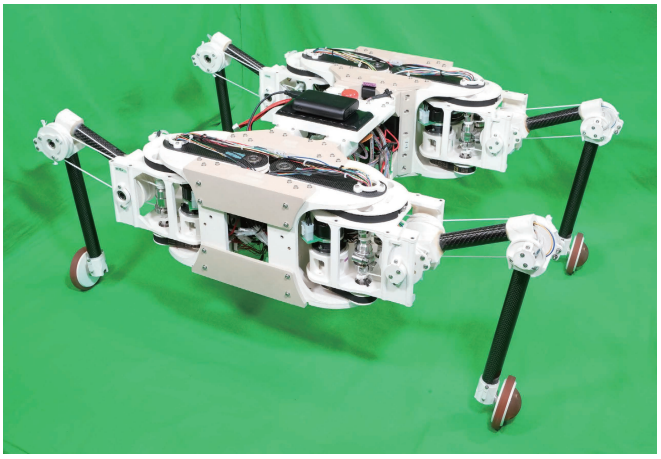

Fig. 1. Roller-Walker II.

TABLE I
Specification of Roller-Walker II

Approximate dimensions (length, width, height)	450, 870, 310 mm,
Length of the each leg link (in order from the body side)	70.0, 165.4, 251.5 mm
Total mass	17.7 kg
Mass of the robot with electrical component	16.4 kg
Mass of ankle switching mechanism per leg	0.2 kg
Mass of all batteries	0.54 kg
Reduction ratio of each joint (in order from the body side)	66.43, 141.84, 141.84

[1]Hana Ito, Akifumi Okubo, Kurumi Osawa, Takahiro Aruga, and Gen Endo are with the Department of Mechanical Engineering, Institute of Science Tokyo, 2-12-1 Ookayama, Meguro-ku, Tokyo 152-8550, Japan Institute of Science Tokyo. ito.h.ay@m.titech.ac.jp

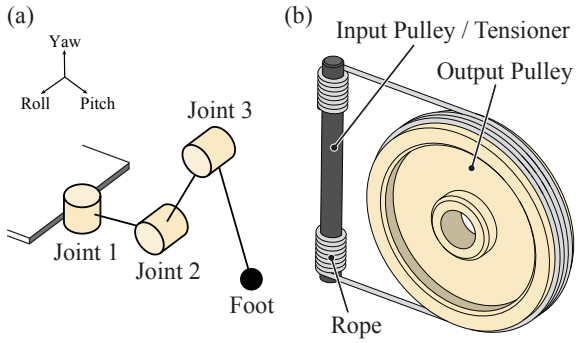

Fig. 2. The leg mechanism of Roller-Walker II. (a) Structure of a leg. (b) Wire drive mechanism for joint 2 and 3.

II. Design of Roller-Walker II

A. Structure

The developed Roller-Walker II is shown in Fig. 1, and its specifications are shown in TABLE I. As shown in Fig. 2(a), it consists of 3 DoF per leg, totaling 12 DoF. The joint 1 is driven by a timing belt, while the joint 2 and 3 use coupled tendon drive with synthetic fiber rope (NA20020SOC00\011.000, heat-set high-density polyethylene fiber, Armare Ropes). Fig. 2(b) shows a schematic diagram of the joint 2 and 3. The shaft around which the rope is wound serves as both the driving shaft and rope tensioner, and is driven from the motor via a timing belt. The tensioning mechanism uses a one-way clutch, which allows the shaft to rotate only in the direction that tightens the rope, enabling easy increase of rope tension [15] [16]. To improve the torque capacity of the tensioning mechanism, a one-way clutch and hose clamp were used in combination [17]. POTICON filament [18], a potassium titanate fiber-reinforced material (NLT34M: nylon-based, RT4: PPS-based, both from Otsuka Chemical Co., Ltd.), was used for main structural components, and those parts fabricated with a 3D printer (G-ZERO, Gutenberg Co., Ltd). The material properties of the filaments used in this study are summarized in Table II. Most of the structural components were fabricated using POTICON filament NTL34M. Among short-fiber-reinforced filaments for fused filament fabrication (FFF), POTICON filament RT4 exhibits, to the best of the authors' knowledge, the highest tensile strength. Although carbon fiber composites such as CFRP offer superior mechanical properties, they are not suitable for the fabrication of geometrically complex components. While carbon short-fiber-filled filaments can also be employed in 3D printing, POTICON filament RT4 demonstrates greater mechanical strength. Accordingly, CFRP was adopted for components that require high strength but have relatively simple geometries, such as leg links. Conversely, for highly loaded components with intricate geometries—specifically, the joints connecting the body and leg mechanisms—POTICON filament RT4 was utilized. This choice takes advantage of the inherent benefits of 3D-printed materials, including low-cost and rapid fabrication of complex structures. The actuators used were brushless

TABLE II
Official material properties of POTICON filaments [18]. All values were measured in accordance with the ISO 178 standard.

NTL34M	X-Y direction	Z-X direction
Bending strength [MPa]	199	107
Flexural Modulus [GPa]	7.0	2.8
RT4	**X-Y direction**	**Z-X direction**
Bending strength [MPa]	210	-
Flexural Modulus [GPa]	9.7	-

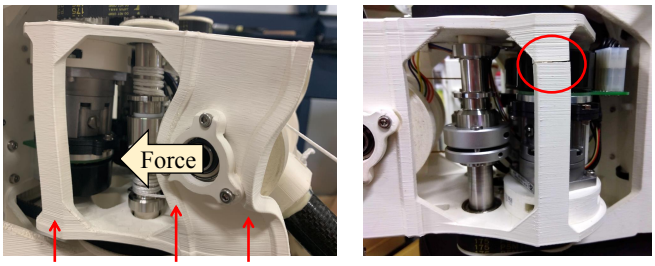

Fig. 3. Deformation of leg components of TITAN-E1. Areas subjected to large forces due to rope tension are significantly deformed. Interlayer delamination, which is often a problem with FFF 3D printers, also occurred.

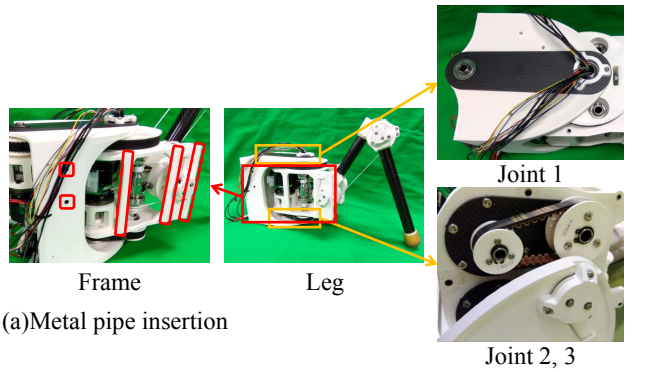

(a)Metal pipe insertion
(b)CFRP sheets installation

Fig. 4. Reinforcement of 3D printed parts.

motors with a rated power of 80 W (591480, maxon) and reducers with a gear ratio of 30 (CSF-14-30-2A-R, Harmonic Drive). For robot operation, a LiFe battery (rated 26.4 V, capacity 1100 mAh, Cosmo Energy) was mounted, and for microcontroller power supply, a lithium-ion battery (Anker PowerCore 10000, rated 5 V, capacity 10000 mAh, ANKER) was installed.

B. Reinforcement for 3D-printed parts

In the walking robot TITAN-E1 [14], which used 3D-printed plastic components as the primary structural material, deformation and cracks occurred in areas subjected to large forces, as shown in Fig. 3. Therefore, to reinforce the 3D-printed plastic components, metal pipes were inserted into the frame columns and wall sections as shown in Fig. 4(a). The effectiveness of this method has been confirmed by previous research [19]. Here, SUS304 pipes with an outer

diameter of $\phi 5.0$ and inner diameter of $\phi 3.0$ were used. Additionally, as shown in Fig. 4(b), CFRP sheets were used to connect two timing pulleys to withstand the tension of timing belts. These reinforcements prevented the plastic from creep deformation and cracking even when subjected to large tensions from wire drive ropes and timing belts.

Furthermore, the printing conditions for plastic components were set with triangular infill patterns and an infill density of 50 % or higher. In particular, the principal load-bearing parts were printed with an infill ratio greater than 90 % to ensure sufficient structural rigidity. These are parameters that have been confirmed to enhance strength in previous research [20]. Additionally, various components were strengthened through techniques such as simply increasing thickness or adding ribs.

C. Ankle switching mechanism

1) Design: The ankle switching mechanism requires the following two conditions:

- It must be able to structurally support the ground reaction forces acting on the leg tips.
- It must not compromise the lightweight characteristic of the leg tips, which is an advantage of Roller-Walker.

The structure of the ankle switching mechanism proposed in this paper is shown in Fig. 5, and adopts a linear motion mechanism using a lead screw. When switching the walking mode, the switching operation is performed with the robot supported on three legs and one leg lifted. When in either the walking mode shown in Fig. 5(a) or the Roller-Walk mode shown in Fig. 5(c), the ankle joint is housed and fixed inside the pipe of the shank link. However, during switching as shown in Fig. 5(b), the leg tip is lifted and the lead screw extends the leg tip, causing the ankle joint to emerge from the pipe and allowing passive rotation of the ankle joint. At this time, due to gravity, the leg tip always points downward regardless of the angle of the shank link.

To transition to the walking mode shown in Fig. 5(a) from this state, the shank link is positioned perpendicular to the ground and then the leg tip is retracted, fixing the leg tip in a downward-pointing state. In walking mode, forces are received between the disc portion of the wheel axle component shown in light blue in Fig. 5(d) and the pipe tip.

On the other hand, to transition to the Roller-Walk mode shown in Fig. 5(c), the leg tip is moved in the direction approaching the body to tilt the shank link, then the leg tip is extended to allow passive rotation of the ankle joint. Subsequently, by retracting the leg tip while keeping the shank link tilted, the light blue wheel axle contacts the pipe tip of the shank link and rotates passively, fixing the leg tip in a 90-degree rotated state. In Roller-Walk mode, forces are received between the light blue wheel axle and the pipe tip. The components at the tip of the shank link shown in red and green in Fig. 5 are parts designed to constrain rotation around the shank link. The green component is bonded to the CFRP pipe of the shank link, and rotation is prevented by engaging the teeth of those components. Ideally, no rotation around the shank link should occur, because the passive wheel does not generate rotational torque. However, this design was adopted to withstand large torques that may be generated when the passive wheel collides with walls or steps.

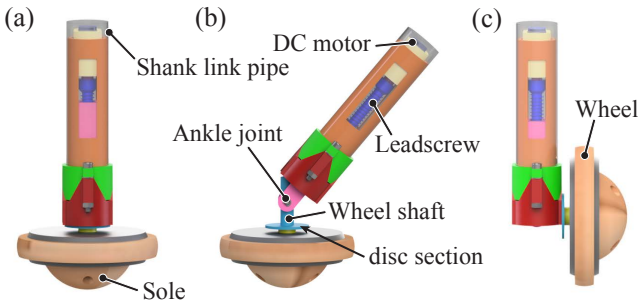

Fig. 5. Ankle switching mechanism.

For the actuator, a small geared motor (Micro Metal Gearmotor HP, gear ratio 75:1, Pololu) was used. In both walking and Roller-Walk cases, when retracted to the limit, the wheel axle component contacts the pipe tip causing the motor to stall. Therefore, the current flowing through the motor is measured using a current sensor (ACS712 High-Sensitivity Current Sensor Module Kit, Akizuki Denshi Tsusho Co., Ltd.), and when the motor stalls and the current value exceeds a certain threshold, the current is cut off to stop the motor.

In this mechanism, as mentioned above, forces are structurally received at the contact point between the wheel axle component shown in light blue in Fig. 5 and the pipe, and ideally the ankle joint and actuator sections do not bear forces. Additionally, the advantage of Roller-Walker is that the leg tips are lightweight without actuators for driving wheels, and the ankle switching mechanism is required to have a design that does not compromise this advantage. The motor for switching leg tips is small and lightweight (9.4 g), which is 0.3 % of the mass of one leg (3700 g), so it is considered that mounting it on the leg tip will not degrade walking performance. Furthermore, the total mass of this mechanism is 173.0 g per leg, which is 4.7 % considering the entire leg, making it a sufficiently small value.

Additionally, the lead screw used in this mechanism was 3D printed with POTICON filament NLT34M (Otsuka Chemical Co., Ltd.). The advantages of using 3D-printed components include being lightweight and allowing free design of the lead screw diameter and lead. In this mechanism, it was designed with $\phi 8$ and a lead of 2 mm. The lead was set sufficiently small to prevent back-driving. Compared to a lead screw made of SUS304 with the same specifications, the mass was reduced to 13.6 %. Additionally, urethane rubber (A50) was used for the wheels and the hemispherical portions of the walking leg tips.

2) Load-bearing test: A prototype of beyond the Joint 3 was fabricated using a CFRP pipe with the same dimensions as that employed in the Roller-Walker II for the shank link. Using this prototype, both static and dynamic load tests were conducted to evaluate its load-bearing capacity.

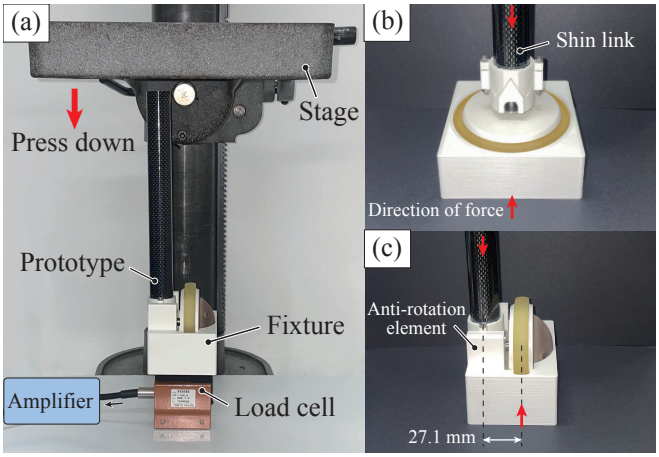

Fig. 6. Static load testing for load-bearing capacity. (a) Experimental setup. (b) Fixture for walking mode. (c) Fixture for Roller-Walk mode.

In addition to experimental approaches, numerical analyses based on finite element modeling could also be considered for estimating durability. However, since the filament used in this study is a nonlinear viscoelastic material and 3D-printed parts exhibit strong anisotropy depending on the build direction, the application of the finite element method becomes highly complex and challenging. Therefore, in this study, the durability was evaluated experimentally through tests conducted on the fabricated prototype.

First, in the static load measurement test, a quasi-static load was applied in the vertical direction. The experimental setup is shown in Fig. 6(a), where the prototype was installed on the lower side of a drill press stage, and force was manually applied by gradually lowering the stage. As shown in Fig. 6(b) and (c), the prototype was fixed using fixtures for walking mode and Roller-Walk mode respectively. The magnitude of the force was measured using a load cell (U3B1-1K-B, rated capacity 980.7 N, MinebeaMitsumi Inc.) and an amplifier (WGA-670B, Kyowa Electronic Instruments Co., Ltd.). As a result, in both walking and Roller-Walk modes, the mechanism did not break even when a force of 980.7 N, which is the rated capacity of the load cell, was applied. Considering that the main body mass is 17.7 kg, this is considered a sufficient value for walking and Roller-Walk locomotion. Since the purpose of the present test was solely to confirm that the structure can withstand sufficient loads as a walking machine, the specimens were not tested up to failure.

Next, in the dynamic load measurement test, the prototype was installed as shown in Fig. 7, and impact force was applied to the leg tip by dropping a weight from above. A 2 kg weight was used, and it was dropped from heights varying from 0.1 m, 0.2 m, ... in 0.1 m increments up to 0.7 m. The direction of impact force application was vertical only for walking mode, and both vertical and x-axis direction (force from the traveling direction) for Roller-Walk mode. As a result, in the walking mode and x-axis direction tests of Roller-Walk mode, the mechanism did not break up to 0.7 m.

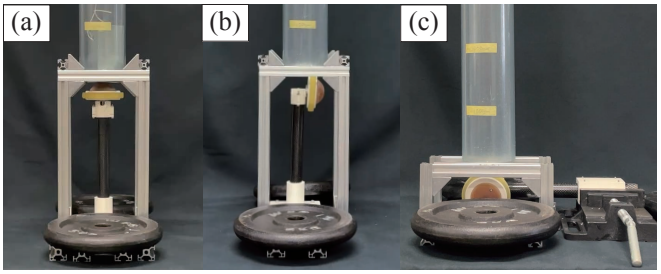

Fig. 7. Setup of load carrying capacity tests on dynamic loads. (a) Vertical direction in walking mode. (b) Vertical direction in Roller-Walk mode. (c) X-axis direction in Roller-Walk mode.

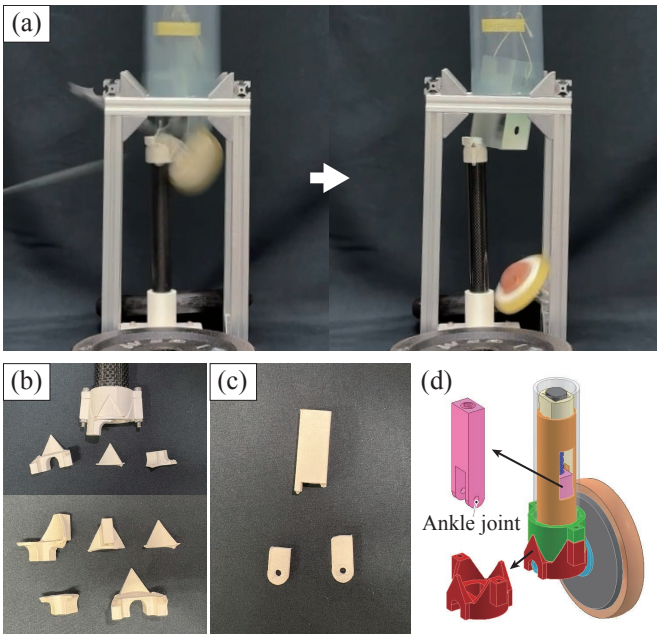

Fig. 8. (a) Fracture of ankle joint when a 2 kg weight is dropped from a height of 0.7 m in a vertical test in roller walk mode. (b)(c) Broken parts. (d) Detail of the broken parts.

However, in the vertical direction of Roller-Walk mode, when the weight was dropped from 0.7 m, the ankle portion broke as shown in Fig. 8(a), resulting in two 3D-printed components splitting. The broken components are shown in Fig. 8(b), and as shown in Fig. 8(c), they are the component at the tip of the shank link pipe that receives force from the wheel axle, and the lead screw nut connected between the wheel axle and ankle joint. Based on this result, the design was modified to increase the thickness of the portion of the former component that directly receives force from the wheel axle. However, even the pre-modification design could withstand the impact of dropping a 2 kg weight from a height of 0.6 m, which is considered sufficient design for walking and Roller-Walk propulsion. The durability under long-term use and harsh environmental conditions should be further investigated over an extended period in the future studies.

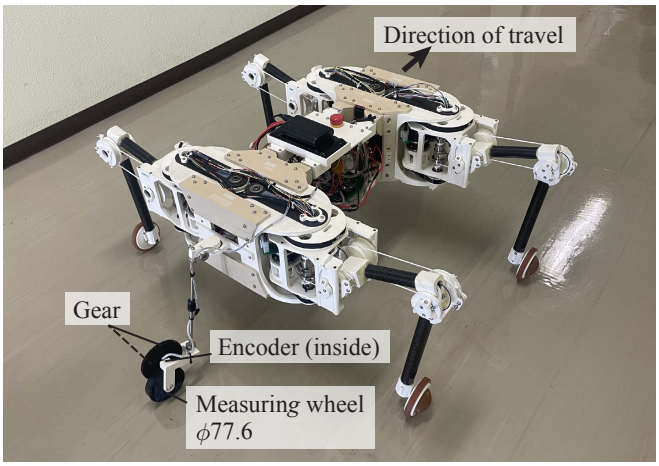

Fig. 9. Velocity measuring wheel attached to the tail side of the body.

III. Locomotion test

Motion verification was conducted for walking and Roller-Walk operations. In the propulsion tests, the Cost of Transport (CoT) during propulsion is considered as an index for performance evaluation. The CoT is a dimensionless quantity expressed by the following equation, where smaller values indicate higher locomotion efficiency [21].

$$\mathrm{CoT} = \frac{E}{MgL} = \frac{P}{MgV} \tag{1}$$

where M [kg] is the total mass of the robot, g [m/s^2] is gravitational acceleration, L [m] is the travel distance, E [J] is the energy consumed for the distance L, P [W] is the power consumption, and V [m/s] is the velocity.

A. Walking

The walking motion is shown in Fig. 10. The walking motion parameters are stance length x_{st}, swing height z_{sw}, velocity in stance phase V_{st}, and duty ratio β. The gait is a crawl gait in which legs are advanced one by one while the body moves at a constant velocity. A lateral swaying motion [22] was added to move the body in the direction of the side where both front and rear legs are in contact with the ground during walking, thereby securing a higher stability margin. Power consumption was calculated from the battery voltage measured before and after operation using a voltmeter and the average current measured using a current sensor (MCS-SD2537, mlabo). Velocity was calculated from encoder values (KP1013C, Sustainable Robotics) by attaching a measuring wheel as shown in Fig. 9. Since it was experimentally found that this encoder cannot measure accurately at high velocities, measurements were taken with a 1/7 gear reduction.

The experiment was conducted on a vinyl floor sheet, achieving stable walking motion. With parameters set to $x_{\mathrm{st}} = 200$ mm, $z_{\mathrm{sw}} = 100$ mm, $V_{\mathrm{st}} = 0.1$ m/s, and $\beta = 0.75$, the velocity was 0.07 m/s and the CoT was 8.45. When corrected by subtracting 21.4 W, which is the power consumption when only servos are operated in the air, the CoT becomes 6.58.

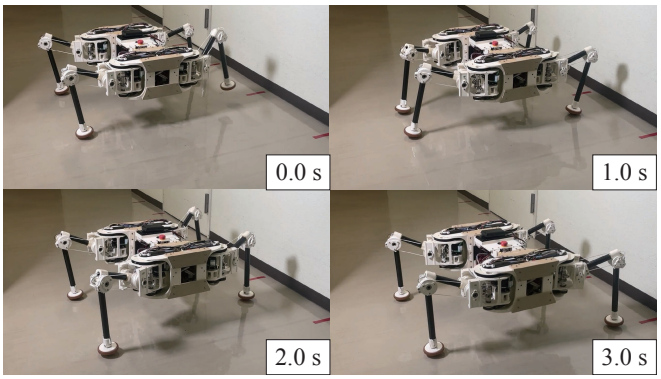

Fig. 10. Locomotion experiment of walking mode using crawl gait.

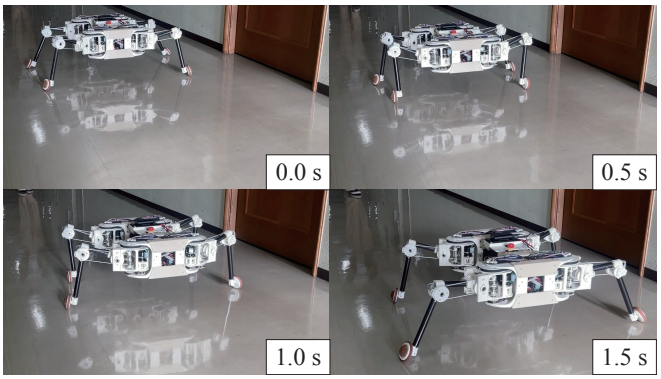

Fig. 11. Locomotion experiment of Roller-Walk mode.

B. Roller-Walk

The propulsion using Roller-Walk is shown in Fig. 11. The leg trajectory is same as that in the literature [9], with parameters including leg trajectory period T, radial initial leg tip position d_{offset}, radial amplitude d_0, circumferential amplitude θ_0, and phase difference between front and rear legs ϕ. The measurement methods for power consumption and velocity are the same as those in the walking propulsion test.

First, as parameters for safe propulsion, $T = 3$ s, $d_{\mathrm{offset}} = 230$ mm, $d_0 = 80$ mm, $\theta_0 = 0.27$, and $\phi = \pi/2$ were set, and a propulsion test was conducted on a vinyl floor. The velocity in this case was 0.60 m/s, and the CoT was 0.83. The corrected CoT after subtracting the power consumption when only servos are operated in the air is 0.63.

Next, an experiment was conducted to measure the maximum speed of propulsion using Roller-Walk by changing the parameters. The experiment is shown in Fig. 12. The experiment was conducted on a hard and flat flooring surface with a 50 m straight distance. However, since large loads were expected on the leg tips in this experiment, the ankle switching mechanism was not installed, and inline skating wheels (ϕ80, thickness 24 mm, RADIOUS) were mounted. In addition to the change in the foot parts, a laptop weighing 1.7 kg was loaded for recording purposes, bringing the total mass of the robot at that time to 19.6 kg. As a result, a maximum speed of 3.43 m/s was recorded when the

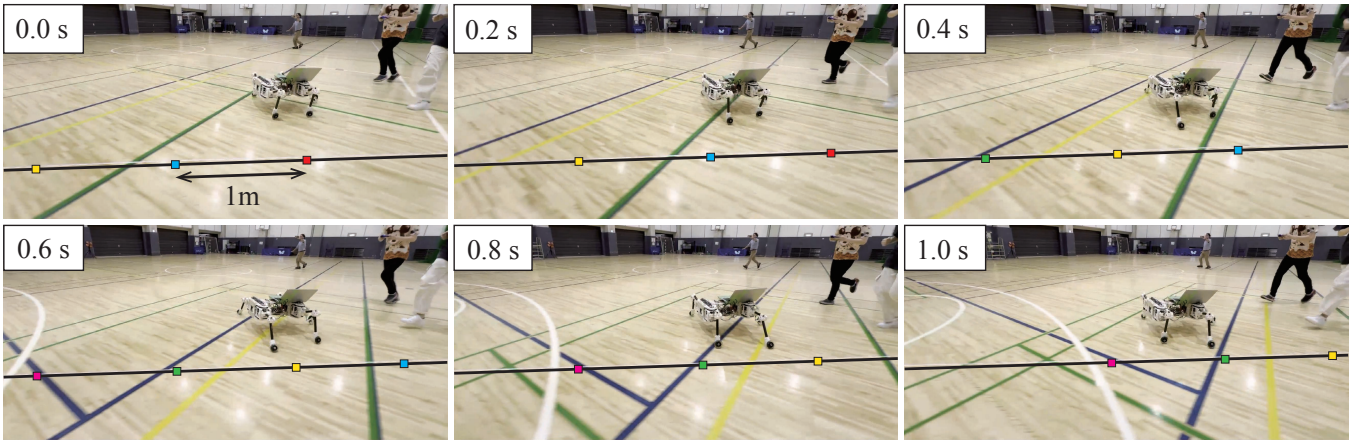

Fig. 12. Maximum velocity measurement experiment. Markers of the same color represent identical positions.

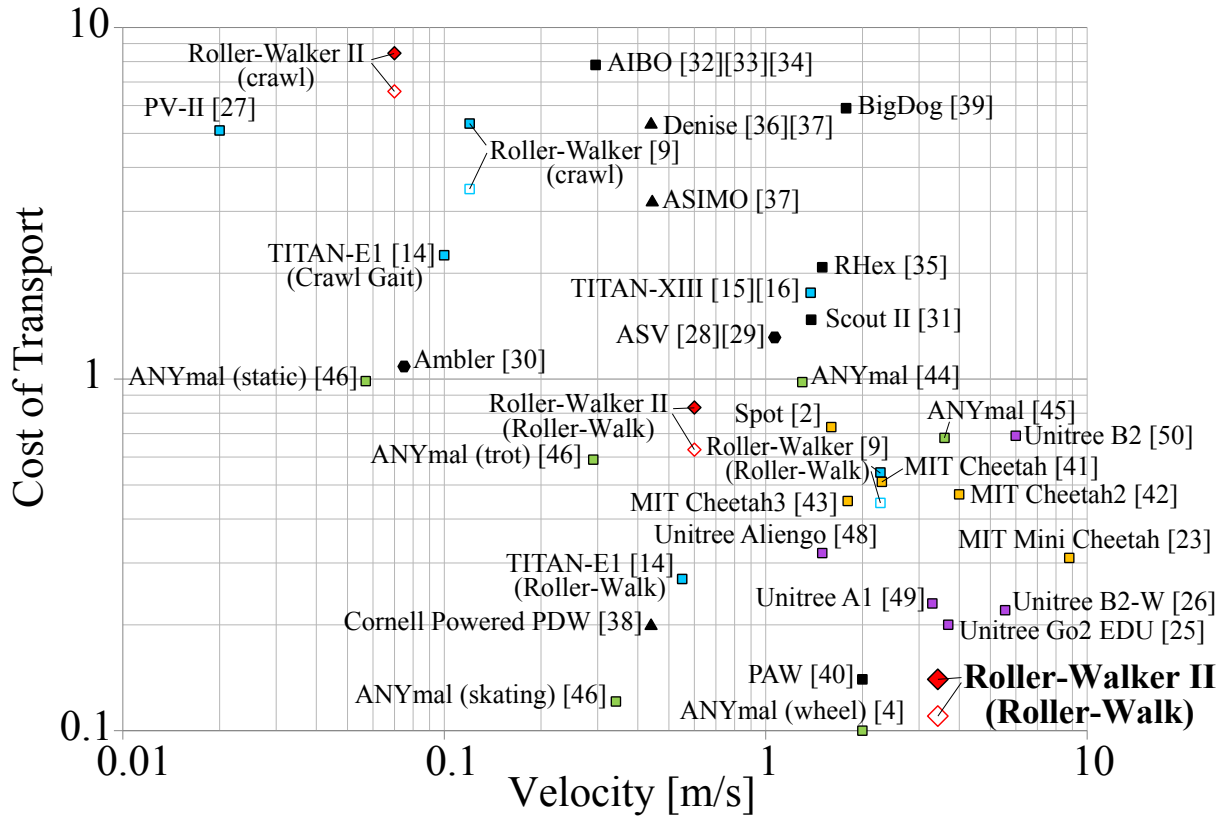

Fig. 13. CoT for various mobile robots. CoT of various mobile robots. Triangles represent bipedal, squares represent quadrupedal, and hexagons represent hexapedal robots. Roller-Walker II is shown in red.

parameters were set to $T = 1.3$ s, $d_{\text{offset}} = 160$ mm, $d_0 = 130$ mm, $\theta_0 = 0.15$, and $\phi = \pi/2$. This result significantly exceeds the maximum speed of the conventional Roller-Walker of 2.27 m/s [9] by 1.16 m/s. The CoT at this time was 0.14. When corrected by subtracting the power consumption when only servos are operated in the air, the CoT becomes 0.11. In future work, high-load experiments will be conducted using the complete configuration equipped with the ankle switching mechanism to verify whether the robot can operate stably at speeds comparable to or higher than those achieved in the present experiments.

IV. Discussion

Fig. 13 shows a comparison of various mobile robots with velocity [m/s] on the horizontal axis and CoT on the vertical axis. In this figure, robots positioned toward the bottom right can be considered to have higher performance as mobile robots. It should be noted that the CoT of each robot is either adopted from explicitly stated values in the literature or estimated using average power consumption calculated from battery capacity and operating time when not explicitly stated. In the walking mode of Roller-Walker II, the velocity

was relatively low at $0.07\ \mathrm{m/s}$, and the CoT was inferior to that of the Roller-Walk mode and other comparable robots. In this experiment, we employed parameters that ensured stable walking; however, further increases in velocity are expected if parameters such as V_{st} (velocity in the stance phase) are optimally tuned. Moreover, considering that the robot achieved only about 70% of the target velocity even when V_{st} was set to $0.1\ \mathrm{m/s}$, there remains room for improvement in the control system, suggesting the potential for further enhancement of waling performance. On the other hand, the CoT of Roller-Walker II at maximum speed during Roller-Walk is 0.14 (0.11), which is confirmed to be highly efficient, comparable to walking robots such as MIT Mini Cheetah [23] [24] and Unitree's Go2 (EDU) [25], as well as the leg-wheeled B2-W [26] and ANYmal with wheel [4]. Among leg-wheeled robots, Roller-Walker II exhibits a lower maximum speed than B2-W, but achieves a superior CoT. This improvement in CoT is considered to result primarily from weight reduction achieved through the use of 3D-printed resin components and passive wheels in the Roller-Walker II. When compared with the ANYmal with wheels, the CoT of the proposed robot was slightly inferior. Although the maximum speed of the ANYmal with wheels has been reported to be $4\ [\mathrm{m/s}]$ [4], the corresponding CoT value has not been disclosed, making direct comparison impossible. We believe that the superiority of Roller-Walker II can be further demonstrated by achieving improved CoT through further speed enhancement and implementing switching between propulsion methods according to ground conditions.

V. Conclusion

A leg-wheeled robot, Roller-Walker II, was developed using 3D-printed plastic as the primary structural components, and locomotion experiments were conducted for walking and Roller-Walk. Particularly in Roller-Walk, a maximum speed of $3.43\ \mathrm{m/s}$ and a CoT of 0.14 were achieved, demonstrating that the robot belongs to the highest performance group compared to other walking robots. In the future, we plan to measure CoT and wheel rolling resistance on various outdoor road surfaces as indicators for switching between walking and Roller-Walk. Based on these data, we will examine the timing for switching and aim to realize terrain-adaptive propulsion. This development is anticipated to facilitate future industrial applications, including exploration, surveillance, and material transportation in real-world environments.

Acknowledgment

In preparing this paper, we received materials, information, and valuable advice from Otsuka Chemical Co., Ltd., as well as cooperation and guidance regarding 3D printing from Gutenberg Co., Ltd. We would like to express our deepest gratitude for their assistance. We also extend our sincere thanks to Prof. Naoyuki Takesue (Tokyo Metropolitan University), Prof. Yusuke Ota (Chiba Institute of Technology), and Prof. Takeshi Takaki (Hiroshima University) for their insightful comments and discussions.

References

[1] P. Biswal and P. K. Mohanty, "Development of quadruped walking robots: A review," *Ain Shams Engineering Journal*, vol. 12, no. 2, pp. 2017–2031, 2021.

[2] Boston Dynamics, "Spot," https://bostondynamics.com/products/spot/, accessed on 30.07.2025.

[3] Hangzhou Yushu Technology Co., Ltd. (Unitree Robotics), "Unitree robots," https://www.youtube.com/watch?v=vG3re3uXTGA, accessed on 30.07.2025.

[4] M. Bjelonic, C. D. Bellicoso, Y. de Viragh, D. Sako, F. D. Tresoldi, F. Jenelten, and M. Hutter, "Keep rollin'–whole-body motion control and planning for wheeled quadrupedal robots," *IEEE Robotics and Automation Letters*, vol. 4, no. 2, pp. 2116–2123, 2019.

[5] M. Bjelonic, "Planning and control for hybrid locomotion of wheeled-legged robots," Ph.D. dissertation, ETH Zurich, 2021.

[6] Kawasaki Heavy Industries, Ltd., "Four-legged walking robot "RHP Bex"," https://www.youtube.com/watch?v=vG3re3uXTGA, accessed on 30.07.2025.

[7] Hangzhou Yunshenchu Technology Co., Ltd. (DEEP Robotics), "DEEPRoboticsLynx," https://www.deeprobotics.cn/en/index/deeproboticslynx.html, accessed on 30.07.2025.

[8] Shanghai Zhiyuan Innovation Technology Co., Ltd. (AgiBot), "AgiBot unveils the X2-N," https://www.youtube.com/watch?v=ZcqBPFZ3n6M, accessed on 30.07.2025.

[9] G. Endo and S. Hirose, "Study on roller-walker –system integration and basic experiments–," *Journal of the Robotics Society of Japan*, vol. 18, no. 2, pp. 270–277, 2000.

[10] P.-A. Léziart, T. Flayols, F. Grimminger, N. Mansard, and P. Souères, "Implementation of a reactive walking controller for the new open-hardware quadruped solo-12," in *IEEE International Conference on Robotics and Automation (ICRA)*, 2021, pp. 5007–5013.

[11] J. Kim, T. Kang, D. Song, and S.-J. Yi, "Design and control of a open-source, low cost, 3d printed dynamic quadruped robot," *Applied Sciences*, vol. 11, no. 9, p. 3762, 2021.

[12] Autodiscovery, "Stella Educational quadruped," https://www.autodiscovery.co.uk/robots/stella.html, accessed on 30.06.2025.

[13] S. E. Schoedel, A. J. Fuge, B. Kalita, and A. Leonessa, "Development of an affordable and modular 3d printed quadruped robot," in *ASME International Mechanical Engineering Congress and Exposition*, vol. 86663. American Society of Mechanical Engineers, 2022, p. V004T06A017.

[14] S. Tsunoda, H. Nabae, K. Suzumori, and G. Endo, "Development of Quadruped Robot TITAN-E1 Using Plastic Structural Parts Printed by Fused Deposition Modeling," in *JSME Conference on Robotics and Mechatoronics*, no. 2A1-Q07, 2022 (in Japanese).

[15] S. Kitano, S. Hirose, G. Endo, and E. F. Fukushima, "Development of lightweight sprawling-type quadruped robot TITAN-XIII and its dynamic walking," in *IEEE/RSJ International Conference on Intelligent Robots and Systems (IROS)*, 2013, pp. 6025–6030.

[16] S. Kitano, S. Hirose, A. Horigome, and G. Endo, "TITAN-XIII: sprawling-type quadruped robot with ability of fast and energy-efficient walking," *Robomech Journal*, vol. 3, pp. 1–16, 2016.

[17] H. Ito, K. Osawa, A. Okubo, and G. Endo, "Basic study for drive mechanism with synthetic fiber rope: Development of a tensioning mechanism using a one-way clutch and hose clamp," in *IEEE/SICE International Symposium on System Integration (SII)*, 2025, pp. 399–404.

[18] Otsuka Chemical Co., Ltd., "POTICON Filament," https://www.otsukac.co.jp/en/products/cat-composite-resin/filament.html, accessed on 07.11.2025.

[19] K. Osawa and G. Endo, "Does thin-walled metal pipe insertion increase the bending strength of 3d printed parts?" in *IEEE/SICE International Symposium on System Integration (SII)*, 2024, pp. 585–591.

[20] ——, "Mechanical parts manufactured by a 3d printer for industrial robot: Relationship between infill pattern, infill density, and printing speed and bending strength of beams," in *The 24th SICE System Integration Division Annual Conference (SI2023)*, no. 1E5-04, 2023 (in Japanese).

[21] G. Gabrielli and T. von Karman, "What price speed? specific power required for propulsion of vehicles," *Mechanical Engineering*, vol. 72, no. 10, pp. 775–781, 1950.

[22] S. Hirose and K. Yoneda, "Dynamic & static control and continuous trajectory generation of quadruped walking vehicle," *Journal of the Robotics Society of Japan*, vol. 3, no. 9, pp. 267–275, 1991.

[23] B. Katz, J. D. Carlo, and S. Kim, "Mini cheetah: A platform for pushing the limits of dynamic quadruped control," in *IEEE International Conference on Robotics and Automation (ICRA)*, 2019, pp. 6295–6301.

[24] G. B. Margolis, G. Yang, K. Paigwar, T. Chen, and P. Agrawal, "Rapid locomotion via reinforcement learning," *The International Journal of Robotics Research*, vol. 43, no. 4, pp. 572–587, 2024.

[25] Hangzhou Yushu Technology Co., Ltd. (Unitree Robotics), "Unitree go2," https://www.unitree.com/go2, accessed on 30.07.2025.

[26] ——, "Unitree b2-w," https://www.unitree.com/b2-w, accessed on 30.07.2025.

[27] S. Hirose and Y. Umetani, "The basic motion regulation system for quadruped walking vehicle," in *ASME Design Engineering Technical Conference*, 1981.

[28] K. Waldron and R. McGhee, "The adaptive suspension vehicle," *IEEE Control Systems Magazine*, vol. 6, no. 6, pp. 7–12, 1986.

[29] D. R. Pugh, E. A. Ribble, V. J. Vohnout, T. E. Bihari, T. M. Walliser, M. R. Patterson, and K. J. Waldron, "Technical description of the adaptive suspension vehicle," *The International Journal of Robotics Research*, vol. 9, no. 2, pp. 24–42, 1990.

[30] E. Krotkov and R. G. Simmons, "Performance of a six-legged planetary rover: power, positioning, and autonomous walking." in *IEEE International Conference on Robotics and Automation (ICRA)*, 1992, pp. 169–174.

[31] S. Talebi, I. Poulakakis, E. Papadopoulos, and M. Buehler, "Quadruped robot running with a bounding gait," in *Experimental Robotics VII*. Springer, 2002, pp. 281–289.

[32] M. S. Kim and W. Uther, "Automatic gait optimisation for quadruped robots," in *Australasian Conference on Robotics and Automation*, 2003, pp. 1–3.

[33] S. Chernova and M. Veloso, "An evolutionary approach to gait learning for four-legged robots," in *IEEE/RSJ International Conference on Intelligent Robots and Systems (IROS)*, vol. 3. IEEE, 2004, pp. 2562–2567.

[34] Sony Group Corporation, "aibo ers-1000 specification," https://helpguide.sony.net/aibo/ers1000/v1/en/contents/TP0001970140.html, accessed on 30.07.2025.

[35] D. Campbell and M. Buehler, "Preliminary bounding experiments in a dynamic hexapod," in *Experimental Robotics VIII*. Springer, 2003, pp. 612–621.

[36] M. Wisse, "Three additions to passive dynamic walking; actuation, an upper body, and 3d stability," in *IEEE/RAS International Conference on Humanoid Robots*, vol. 1, 2004, pp. 113–132.

[37] S. Collins, A. Ruina, R. Tedrake, and M. Wisse, "Efficient bipedal robots based on passive-dynamic walkers," *Science*, vol. 307, no. 5712, pp. 1082–1085, 2005.

[38] S. Collins and A. Ruina, "A bipedal walking robot with efficient and human-like gait," in *Proceedings of the 2005 IEEE International Conference on Robotics and Automation*, 2005, pp. 1983–1988.

[39] M. Raibert, K. Blankespoor, G. Nelson, and R. Playter, "Bigdog, the rough-terrain quadruped robot," *IFAC Proceedings Volumes*, vol. 41, no. 2, pp. 10 822–10 825, 2008.

[40] J. A. Smith, I. Poulakakis, M. Trentini, and I. Sharf, "Bounding with active wheels and liftoff angle velocity adjustment," *The International Journal of Robotics Research*, vol. 29, no. 4, pp. 414–427, 2010.

[41] S. Seok, A. Wang, M. Y. Chuah, D. Otten, J. Lang, and S. Kim, "Design principles for highly efficient quadrupeds and implementation on the mit cheetah robot," in *IEEE International Conference on Robotics and Automation (ICRA)*, 2013, pp. 3307–3312.

[42] H.-W. Park, P. M. Wensing, and S. Kim, "High-speed bounding with the mit cheetah 2: Control design and experiments," *The International Journal of Robotics Research*, vol. 36, no. 2, pp. 167–192, 2017.

[43] G. Bledt, M. J. Powell, B. Katz, J. Di Carlo, P. M. Wensing, and S. Kim, "Mit cheetah 3: Design and control of a robust, dynamic quadruped robot," in *IEEE/RSJ International Conference on Intelligent Robots and Systems (IROS)*, 2018, pp. 2245–2252.

[44] IEEE ROBOTS, "Anymal," https://robotsguide.com/robots/anymal, accessed on 30.07.2025.

[45] M. Hutter, C. Gehring, D. Jud, A. Lauber, C. D. Bellicoso, V. Tsounis, J. Hwangbo, K. Bodie, P. Fankhauser, M. Bloesch, R. Diethelm, S. Bachmann, A. Melzer, and M. Hoepflinger, "Anymal - a highly mobile and dynamic quadrupedal robot," in *IEEE/RSJ International Conference on Intelligent Robots and Systems (IROS)*, 2016, pp. 38–44.

[46] M. Bjelonic, C. Dario Bellicoso, M. Efe Tiryaki, and M. Hutter, "Skating with a force controlled quadrupedal robot," in *IEEE/RSJ International Conference on Intelligent Robots and Systems (IROS)*, 2018, pp. 7555–7561.

[47] ANYbotic, "Anymal," https://www.anybotics.com/robotics/anymal/, accessed on 30.07.2025.

[48] Hangzhou Yushu Technology Co., Ltd. (Unitree Robotics), "Unitree aliengo," https://www.unitree.com/aliengo, accessed on 30.07.2025.

[49] ——, "Unitree a1," https://www.unitree.com/a1, accessed on 30.07.2025.

[50] ——, "Unitree b2," https://www.unitree.com/b2, accessed on 30.07.2025.